Chemistry Europe
European Chemical Societies Publishing

Polyester-ZrO_2 Nanocomposite Electrolytes with High Li Transference Numbers for Ambient Temperature All-Solid-State Lithium Batteries

Tian Khoon Lee,[a, b] Rassmus Andersson,[a] Nurul Akmaliah Dzulkurnain,[a] Guiomar Hernández,[a] Jonas Mindemark,[a] and Daniel Brandell*[a]

Polyester- and polycarbonate-based polymer electrolytes have attracted great interest after displaying promising functionality for solid-state Li batteries. In this present work, poly(ε-caprolactone-*co*-trimethylene carbonate) electrolytes are further developed by the inclusion of ZrO_2 particles, prepared by an *in situ* sol-gel method. SEM micrographs show that the ZrO_2 particles are uniform and 30–50 nm in size. Contrary to many studies on filler-polymer electrolytes, the changes in ionic conductivity are less significant upon addition of zirconia filler to the polymer electrolyte, but remain at $\sim 10^{-5}$ S cm^{-1} at room temperature. This can be explained by the amorphous nature of the polymer. Instead, high lithium transference numbers (0.83–0.87) were obtained. Plating/stripping tests with Li metal electrodes show long-term cycling performance for >1000 cycles at 0.2 mA cm^{-2}. Promising solid-state lithium battery cycling results at ambient temperature using the material are also shown.

1. Introduction

Since the commercialization of the lithium-ion battery (LIB) by SONY in 1991,[1–2] this battery technology has experienced rapid growth and several leaps in its development. Today, LIBs appear in a range of sizes, from megawatt packs which store power from solar farms, down to miniaturized applications in electronic watches or pacemakers. Last year, this remarkable development was crowned by the Nobel Prize in Chemistry, awarded John B. Goodenough, M. Stanley Whittingham, and Akira Yoshino.[3]

Lithium metal is often being envisaged as an ultimate anode for high energy density LIBs. Lithium has the highest theoretical capacity (3860 mAh g^{-1}, equivalent to a specific energy of 387 Wh kg^{-1}) and possesses the lowest electrochemical potential (−3.04 V *vs.* the hydrogen electrode) of all possible Li-based alternatives.[4] Moreover, Li metal is also in focus for so-called next generation Li–O_2 (13000 Wh kg^{-1}) and Li–S (2600 Wh kg^{-1}) batteries, with considerably higher specific energy than in LIBs.[5–6] However, lithium metal poses several drawbacks when used as anode: poor safety features and cyclability, especially when a flammable liquid organic electrolyte is used. Therefore, solid-state lithium batteries (SSBs) which utilize solid-state electrolytes (SSEs) are highly desired. These enable higher energy density, longer cycle life, no electrolyte leakage, possess high thermal stability and often high electrochemical stability.[7] Generally, SSEs can be divided into two categories: ceramic electrolytes and polymer electrolytes. Their properties differ considerably; while ceramic electrolytes can possess comparably high bulk conductivity, solid polymer electrolytes (SPEs) often need to be operated at elevated temperature (e.g. 60 °C) to achieve sufficiently high enough conductivity (>10^{-3} S cm^{-1}).[8] In terms of mechanical and structural properties, SPEs are often soft, elastic and non-brittle materials and exhibit isotropic ion conductivity, which are beneficial for battery devices where the electrode particles change in volume and orientation during the charge-discharge process.[8] From an industrial perspective, SPEs are also appealing due to reduce requirement on packaging, state-of-charge monitoring circuits which made easier for production comparing to Li-ion batteries with liquid electrolytes. Likewise, cost-effectiveness in fabrication processes and structural design is highly sought-after.[9] However, the low ionic conductivity of SPEs and the resulting high interfacial resistance between the electrode and the solid electrolyte in LIBs renders obstacles for large-scale commercialization.[7,10–12]

Poly(ethylene oxide) (PEO) is by far the most studied polymer host for SPEs, attributed to its strong Li^+ solvating capabilities. It is the only polymer which has been used for commercial SSBs, but is nevertheless not widely employed.[13] PEO-based electrolytes possess several inherent limitations, primarily the linked features of high crystallinity and low room temperature ionic conductivity (10^{-6}–10^{-8} S cm^{-1}).[14] PEO-

[a] Dr. T. K. Lee, R. Andersson, Dr. N. A. Dzulkurnain, Dr. G. Hernández, Dr. J. Mindemark, Prof. D. Brandell
Department of Chemistry – Ångström Laboratory
Uppsala University
Box 538, SE-751 21 Uppsala, Sweden
E-mail: daniel.brandell@kemi.uu.se
[b] Dr. T. K. Lee
Department of Chemical Sciences,
Universiti Kebangsaan Malaysia (UKM)
43600, Bangi, Selangor, Malaysia

Supporting information for this article is available on the WWW under https://doi.org/10.1002/batt.202000254

based LIBs therefore need elevated temperature (60 °C), which is above the melting temperature (T_m) of the material, to operate, thereby sacrificing the mechanical properties of the material and becoming insufficient for maintaining its structural integrity.

Another polymeric alternative host for a soft SPE - thereby displaying compatibility with the electrodes - with ion conductive functionalities at room temperature is highly sought-after. In this context, polyesters such as poly(ε-caprolactone) (PCL) and polycarbonates such as poly(trimethylene carbonate) (PTMC) have recently been extensively studied.[15–21] PCL, a semi-crystalline but flexible low-T_g polyester, mimics several properties of PEO as an SPE host and can straight-forwardly be amorphized through copolymerization with PTMC, rendering for example P($CL_{80}TMC_{20}$).[16,20] The corresponding SPEs possess appealing room temperature conductivity properties. However, these materials exhibit poor mechanical properties and pose difficulties in both handling and long-term cycling operation when incorporated into battery cells. In order to mitigate the above issue, incorporating nanoparticles into the polymer electrolyte is generally an effective approaches. A number of nano-particles can be used to improve different properties in SPEs: Al_2O_3, SiO_2, TiO_2, etc. Of these, ZrO_2 have shown promising performance in electrochemical cells in terms of stability, lithium transference numbers and achievable capacities.[22–23] The use of ZrO_2 as the choice for ceramic filler is also further motivated by its straight-forward implementation into SPEs using *in situ* synthesis, which provide good possibilities for avoiding particle agglomeration, which is often a result of dispersion through solvent-casting.[24–25]

In this present work, we therefore focus on the electrochemical properties by incorporating zirconia nanoparticles into the polymer electrolyte matrix of P($CL_{80}TMC_{20}$) SPE.[14–15] Contrary to the conventional strategy of incorporating ready-made nanoparticles into the polymer, these nanocomposite electrolytes are prepared by a one-pot procedure employing an *in situ* sol-gel method.[24–25] It is seen that the soft P($CL_{80}TMC_{20}$)–$LiTFSI_{0.28}$–ZrO_2 is functional for usage in LIBs and can be operated at ambient temperature. Additionally, the electrolytes present good cycling stability and exhibit surprisingly high lithium transference numbers at room temperature, as compared to filler-free electrolyte counterparts.

2. Results and Discussion

2.1. Morphology

Nanocomposite polymer electrolyte (NCPE) materials were synthesized via a one-pot synthesis where the ZrO_2 particles were obtained *in situ* from precursors of zirconium (IV) propoxide, as described in the methodology section. Salt was added in different amounts in acetonitrile solvent. This resulted in a range of samples where the LiTFSI concentration and filler contents varied in the ranges 20–36 wt.% and 1–6 wt.%, respectively.

Figure 1a displays a photo of a representative P($CL_{80}TMC_{20}$)–$LiTFSI_{0.28}$–ZrO_2 (4 wt.%) film. This NCPE material presents the characteristics of a smooth, translucent, soft, and somewhat sticky film, similar to that of a rubbery polymer. No phase separation was observed by visual inspection. To better study the dispersion and distribution of the small particles in the soft polymer matrix, the P($CL_{80}TMC_{20}$)–$LiTFSI_{0.28}$–ZrO_2 was subjected to FIB-SEM, in which a combination of an electron beam and an ion beam are focused and scanned on the same sample area.[26] With this technique, a small volume (with an area in the size of tens of microns) from the surface of the NCPE material is removed by the ion beam to form a pool-shaped cavity. Once the cavity was created, shown in Figure 1b, the nanofillers and its distribution in the polymer matrix could be observed by SEM at the cavity walls. From the micrograph images (Figure 1b–c), it is seen that the matrix of the NCPE is smooth and the nanoparticle of zirconia are 30–50 nm in size and embedded in the polymer, thereby indicating a successful synthesis strategy. The nanoparticles appear well-distributed in the NCPE, and no agglomeration was observed. This further proves that a well-controlled sol-gel reaction can mitigate the agglomeration of nanoparticles as compared to the more conventional method of adding ready-made fillers directly during solution casting.[25] The roughness of the polymer observed in Figure 1b is caused by the milling process, which result in heating damage, redeposition of material and 'curtain effects.[26] To fully confirm that the nanoparticles formed inside the NCPEs were indeed zirconia, similar particles were also synthesized using the same method and conditions as above but without addition of P($CL_{80}TMC_{20}$). Micrographs of these zirconia particles are shown in Figure S1. By comparison, it can be seen that the zirconia nanoparticles in the polymer film are indeed successfully synthesized, with uniform size distribution and without any observable agglomeration. It can thereby be

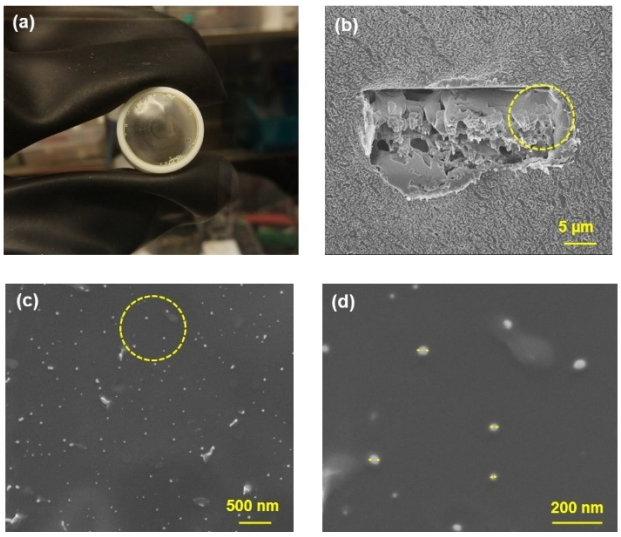

Figure 1. Photograph and SEM micrographs of P($CL_{80}TMC_{20}$)–$LiTFSI_{0.28}$–ZrO_2 (4 wt.%) obtained from FIB-SEM: a) NCPE film after the drying process, b) pool-shaped cavity from milling the surface of the film, c) zirconia nanoparticles at the walls of the cavity, circled in (b), and (d) an enlarged image of the SEM micrograph, circled in (c).

concluded that this facile and straightforward *in situ* method for synthesizing the filler nanoparticles is successful, which could potentially save energy and time, hence reducing the production cost.

2.2. Thermal Analysis

Figure 2 displays the changes in the glass transition temperature between the different studied NCPE materials obtained from the DSC thermograms (found in Figure S2). The DSC data indicate that pure P($CL_{80}TMC_{20}$) has a glass transition temperature (T_g) at −57 °C. For polymer electrolytes containing lithium salt, i.e. P($CL_{80}TMC_{20}$)–LiTFSI with 20 wt.% of LiTFSI salts, an endothermic peak at 25 °C can be observed. The appearance of this T_m peak indicates semi-crystallinity in the electrolyte. This peak appears due to the ε-caprolactone part in the P($CL_{80}TMC_{20}$) copolymer, which has a melting temperature at ca. 55 °C.[20] For the electrolyte comprising 28 and 36 wt.% of LiTFSI, only a T_g peak is observed, which indicate that the addition of salt prevents crystallization. In addition, increasing the salt content increases the T_g value of the polymer electrolyte from −57 to −44 °C, as shown in Figure 2. This is due to that salt-polymer interactions cause the formation of transient cross-links which stiffen the polymer. Interestingly, upon introducing zirconia filler into P($CL_{80}TMC_{20}$)–LiTFSI at various lithium salt contents, two different trends can be seen in the results. At 20 wt.% of LiTFSI salt, increasing zirconia contents reduce the T_g and the intensity of the T_m peak is diminishing. The reverse trend for the glass transition temperature at this salt concentration is related to crystallinity effects, where the presence of crystallites has the effect of increasing the T_g. Obviously, the nanoparticles have a plasticizing effect, preventing crystallization (seen in the DSC curves in Figure S2). At higher salt contents, on the other hand, the opposite trend is observed, i.e. increased T_g with increasing nanoparticle content.

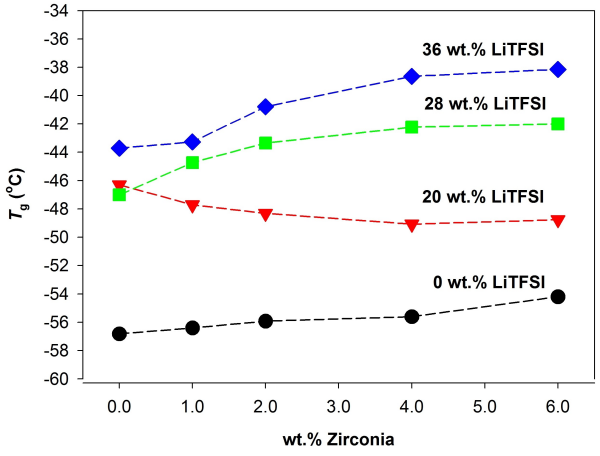

Figure 2. T_g *vs* wt.% of zirconia for P($CL_{80}TMC_{20}$)–$LiTFSI_x$–ZrO_2 samples.

2.3. Molecular Weight and Rheological Properties

The effects of the zirconia synthesis on the molecular weight of P($CL_{80}TMC_{20}$) was investigated by GPC, and the data can be found in Table 1. The molecular weight (M_n) of the filler-free P($CL_{80}TMC_{20}$) copolymer is ca. 225,000 g/mol, but with a relatively high polydispersity. The obtained molecular weight is in good agreement with previous reported data.[20] However, the M_n of the polymers in the NCPEs decreases significantly when the nanoparticles are incorporated, being the lowest for an addition of 6 wt.% of ZrO_2. This implies that the synthesis of the nanoparticles causes some breakdown of the polymer chains, possibly through a hydrolysis process during the sol-gel reaction. The general decrease in M_n of the polymer resulting from the nanoparticle synthesis would correspond to a higher number of shorter chains and hence, increase of the free volume in the resulting material with a concomitant lowering of the T_g. This, however, is not what we observe in the DSC data in Figure 2. Instead, it appears that the zirconia nanoparticles in these amorphous materials primarily act as cross-linking centers for the polymer segments and increase the overall structural stiffness.[30] Consequently, we observe much more robust mechanical properties in these materials than what would otherwise be expected given the limited molecular weights.

The changed molecular weight and morphology with the added nanoparticles is also reflected in the rheological properties of the materials. Figure 3 presents time-temperature superposition master curves of G' and G'' versus frequency measured at 25–100 °C. These frequency sweeps were performed to study the viscoelastic properties of the samples when thermally activated.[28] As seen in Figure 3a, the P($CL_{80}TMC_{20}$)–$LiTFSI_{0.28}$ sample appears solid at room temperature and remains dimensionally stable in a solid-like state down to an angular oscillation frequency of 0.0016 rad s^{-1} when a cross-over is observed; i.e., the elastic modulus (G') is well-below the viscous modulus (G'').[29] On the other hand, the P($CL_{80}TMC_{20}$)–$LiTFSI_{0.28}$–ZrO_2 samples display a much stronger frequency dependence of the moduli. While the cross-over is not seen to shift by a large degree, the nanoparticle-containing samples are seen to soften to a much larger degree when the temperature is increased. When studying the P($CL_{80}TMC_{20}$)–$LiTFSI_{0.28}$–ZrO_2 samples, it is also worth noting that the trend in G' magnitude is similar to the trend in T_g (glass

Table 1. Molecular weights for P($CL_{80}TMC_{20}$)–$LiTFSI_{0.28}$ at various zirconia nanoparticle contents.

Sample	M_n [g/mol]	M_w [g/mol]	PDI
P($CL_{80}TMC_{20}$)–$LiTFSI_{0.28}$ (blank)	224,534	429,449	1.91
P($CL_{80}TMC_{20}$)–$LiTFSI_{0.28}$–ZrO_2 (2 wt. %)	26,218	55,850	2.13
P($CL_{80}TMC_{20}$)–$LiTFSI_{0.28}$–ZrO_2 (4 wt.%)	20,520	39,601	1.93
P($CL_{80}TMC_{20}$)–$LiTFSI_{0.28}$–ZrO_2 (6 wt. %)	16,711	32,623	1.95
P($CL_{80}TMC_{20}$)–$LiTFSI_{0.28}$–ZrO_2 (8 wt. %)	20,752	40,788	1.97

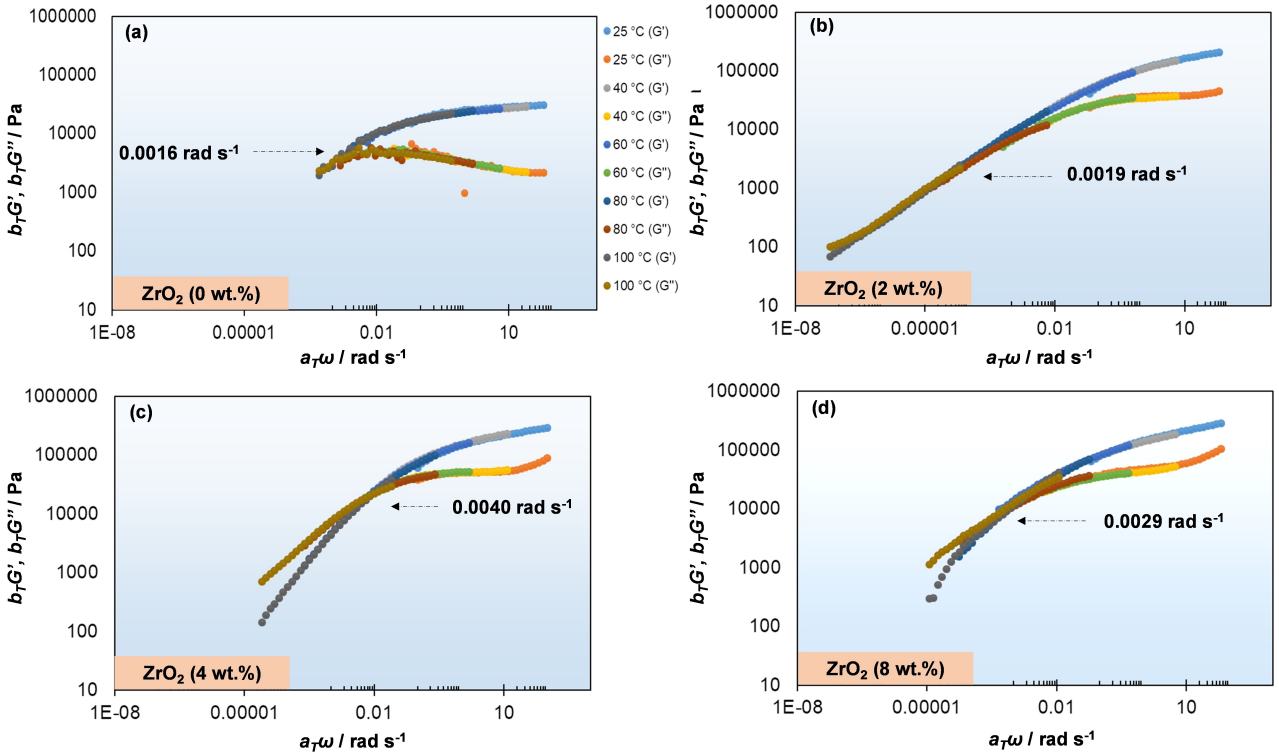

Figure 3. Rheological frequency sweep test (*G′* and *G″ vs* frequency) for temperatures 25–100 °C (reference temperature 25 °C) of P($CL_{80}TMC_{20}$)–$LiTFSI_{0.28}$–ZrO_2 at various concentrations of zirconia nanoparticles. Temperature is indicated as different colors. The cross-over frequency of *G′* and *G″* is indicated for each master curve. The a_T-shift plots are shown in Figure S3.

transition temperature increases with addition of filler; see discussion above), and has higher magnitude of *G′* compared to the filler-free sample.

2.4. Electrochemical Evaluation

2.4.1. Ionic Conductivity

High ionic conductivity is a prerequisite for almost any electrolyte, and one of the key performance parameters when designing SPEs. A common strategy to enhance the ionic conductivity of SPEs is with addition of nano-filler.[27,30] Therefore, the effect of zirconia nanoparticles on the ionic conductivity at various temperatures and salt concentrations was studied using electrochemical impedance spectroscopy on SS/NCPE/SS cells; the results are shown in Figure 4. In Figure 4a, a typical Vogel-Fulcher-Tammann (VFT) type of behavior is seen for the ionic conductivity, indicating that the ionic transport is coupled to polymer segmental motion. This is typically seen in amorphous SPEs and is supported by the DSC results (see discussions above), in which no true melting process is observed. At 30 °C, the overall highest ionic conductivity value was 1.7×10^{-5} S cm^{-1} and achieved for P($CL_{80}TMC_{20}$)–$LiTFSI_{0.28}$–ZrO_2 (4 wt.%). This is a slight improvement of the ionic conductivity of 9.8×10^{-6} S cm^{-1} for the corresponding filler-free SPE P($CL_{80}TMC_{20}$)–$LiTFSI_{0.28}$. Both Wei and Scrosati have found similar trend using ZrO_2 in different polymer hosts.[22–23] The relationship between filler content and conductivity at this temperature can be seen in Figure 4b, where it can be observed that the inclusion of zirconia nanoparticle in these polyester/polycarbonate polymer electrolytes does not have any significant influence on the ionic conductivity. Interestingly, neither does the reduced molecular weight of the polymers as a result of the synthesis seem to influence the conductivity much either. This can be compared to previously reported results for, for example, polyacrylonitrile-$LiClO_4$–LLTO[12], $PEC_{0.53}$–LiFSI–TiO_2,[31] PEO–$LiClO_4$–TiO_2 (or Al_2O_3)[32] and PEO–$LiClO_4$–LATP,[33] which display significantly higher conductivities by addition of nanoparticles.

At lower salt concentration (20 wt.%), an increase in conductivity can be seen with addition of low amounts of zirconia (2 wt.%), but decreasing again for higher filler loadings. In contrast, at higher salt content, the ionic conductivity dropped upon inclusion of ZrO_2 but then increased and reached its highest level at 4 wt.% filler content. The increase in ionic conductivity at 4 wt.% filler content can be related to the maximum "plasticizing" effect, seen in the rheology results. These variations are somewhat more pronounced at the highest salt content studied, i.e. 36 wt.%. An explanation for the more significant increase of ionic conductivity for the 20 wt.% salt sample can be related to a decrease of the crystalline phase,[15] which exists to a limited degree in the pristine P($CL_{80}TMC_{20}$) material. The crystalline peaks seen in the DSC results (discussed above) are indeed diminishing with salt and zirconia content. At 28 wt.% of salt loading and above, the

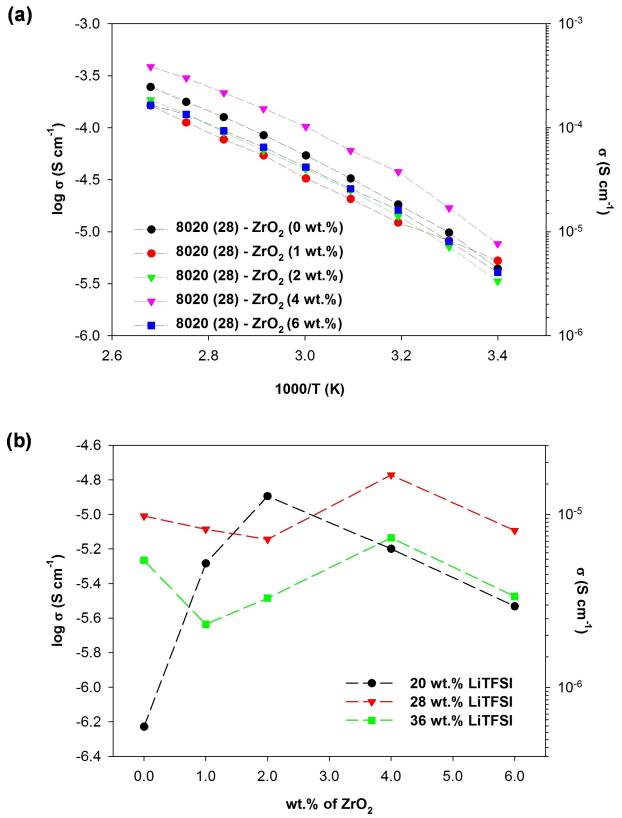

Figure 4. Ionic conductivities for a) $P(CL_{80}TMC_{20})$–$LiTFSI_{0.28}$ with different wt.% zirconia nanoparticles and b) graph of ionic conductivities at 30 °C. Corresponding plots for 20 wt.% of LiTFSI and 36 wt.% of LiTFSI is shown in Figure S4.

crystalline peak disappeared, most probably due to plasticizing effect from the salt. The observed decrease of the ionic conductivity by higher filler loadings for higher salt content samples may be due to stiffening of polymer backbones caused by filler-polymer interactions. This is also supported by the DSC data, in which T_g increases with zirconia content. Thereby, zirconia addition is seen to have less of an influence on the fully amorphous SPEs, i.e. for $P(CL_{80}TMC_{20})$–$LiTFSI_{0.28}$ and $P(CL_{80}TMC_{20})$–$LiTFSI_{0.36}$. This could be expected, since there cannot, for these electrolytes, be any effect of increasing the content of the ion-conducting phase through the prevention of crystallization.

Moreover, a comparison of the ionic conductivity of $P(CL_{80}TMC_{20})$–$LiTFSI_{0.28}$–ZrO_2 (4 wt.%) samples prepared by either *ex situ* or *in situ* methods was performed, and the data is shown in Figure S5 and Figure S6. An ionic conductivity of 5.6×10^{-6} S cm^{-1} was obtained for samples prepared by the *ex situ* method, which is lower than that of sample prepared by the *in situ* method. This difference can be attribute to a better dispersion and size distribution of the obtained nanoparticles.

2.4.2. Lithium Stripping and Plating

Galvanostatic lithium plating/stripping measurements were performed in symmetrical Li/NCPE/Li cells to determine the interfacial stability and charge transfer behavior at the electrode-electrolyte interface, which can affect the overall lifetime of any lithium-battery cell. Considering that long-term ageing of lithium metal polymer cells is of utmost importance, we have performed more than 1000 cycles (totaling up more than 2000 hours of testing). The results (Figure 5a-b) demonstrate that the voltage hysteresis is relatively more stable and lower throughout the cycling in the cell comprising $P(CL_{80}TMC_{20})$–$LiTFSI_{0.28}$–ZrO_2 (4 wt.%) as compared to the filler-free counterpart. Notably, both filler-containing and filler-free SPEs are relatively stable (without significant increase in over-voltage) for such long-term cycling. For the hybrid electrolyte, however, the cell displays a much lower voltage fluctuation, indicating a uniform Li deposition with a stable SEI layer, thereby implying a lower Li^+ transportation resistance and

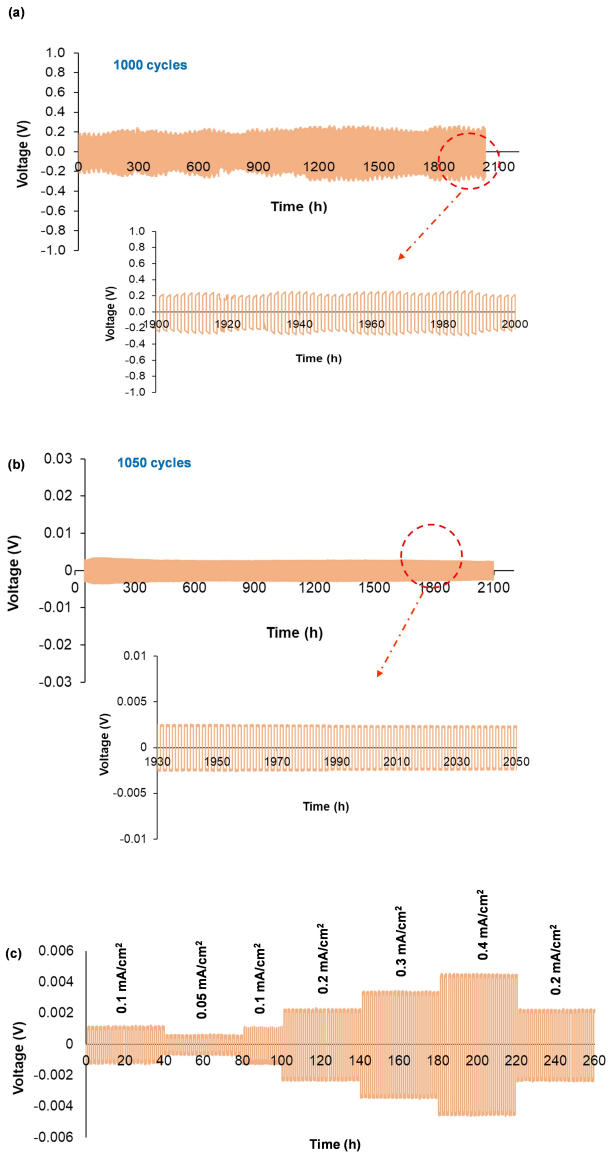

Figure 5. Lithium stripping/plating tests for a) $P(CL_{80}TMC_{20})$–$LiTFSI_{0.28}$ (no filler), b) $P(CL_{80}TMC_{20})$–$LiTFSI_{0.28}$–ZrO_2 (4 wt.%) at a current density of 0.2 mA cm^{-2} and (c) $P(CL_{80}TMC_{20})$–$LiTFSI_{0.28}$–ZrO_2 (4 wt.%) at varying current densities (0.1–0.4 mA cm^{-2}).

good charge transfer kinetics. Further tests were performed to determine the reversibility of lithium stripping/plating of the NCPE at different current densities. It can be seen (Figure 5c) that the cell was able to go up to 0.4 mA cm^{-2}, and that the overvoltage reversibly decreases when lowering the current back to 0.2 mA cm^{-2} at ambient temperature. These results are reproducible (as shown in Figure S7). It can then be assumed that this NCPEs can be safely used at 0.2 mA/cm^2. This is a competitive value for a solid-state electrolyte system, which can assure good durability and safe operation of NCPEs in lithium metal cells. In this context, the low polarization value also indicates an uniform lithium plating/stripping process during the cycling process and the formation of a stable, smooth, and thin SEI layer which prevents further electrolyte decomposition. It would be important to further study the influence of zirconia nano-particles on the formation of the SEI layer, but any in-depth study using (for example) X-ray photo-electron spectroscopy (XPS) was impossible to conduct due to the stickiness of the electrolyte on the electrode.

2.4.3. Li-Ion Transport

Figure 6 shows data for determining the cation ion transference number (T_+), which was obtained by DC polarization combined with EIS at room temperature. It is important to note that, practically, a high total ionic conductivity itself does not guarantee an efficient LIB performance. To accommodate rapid ion transport and avoid concentration polarization, a high T_+ value is desired. Prior to the potentiostatic polarization test, the Li symmetrical cell comprising the optimized NCPE was first stabilized and equilibrated by monitoring the impedance spectrum with respect to time. From Figure 6a, it is seen that the diameter of the high-frequency arcs which corresponds to the charge transfer resistance at the electrode-electrolyte interface (R_{CT}) increased over time and gradually became stable. The spectrum after 6 days of storage coincides with the spectrum of the 7th day, demonstrating good compatibility of P($CL_{80}TMC_{20}$)–$LiTFSI_{0.28}$–ZrO_2 (4 wt.%) with lithium, and that the lithium surface is properly passivated. Furthermore, the bulk resistance (R_b) remained unchanged throughout the storage period. As shown in Figure 6b, the R_{CT} impedance after polarization remained unchanged after the current reached a steady state of 1.05 μA cm^{-2} from the initial value of 1.13 μA cm^{-2}. This corresponds to a remarkable T_+ of 0.83–0.87 for the P($CL_{80}TMC_{20}$)–$LiTFSI_{0.28}$–ZrO_2 (4 wt.%) electrolyte at room temperature (the measurements were repeated 3 times with a new batch of NCPE; see Figure S8), which far exceeds most of any transference numbers reported for SPEs in literature.[20,25,31,34–36] In our previous work, P($CL_{80}TMC_{20}$)–$LiTFSI_{0.36}$ without nano-filler displays a T_+ of 0.66 and 0.62 at 60 °C and 40 °C, respectively.[20] While Tominaga and co-workers reported a similarly high lithium transference number value for their $PEC_{0.53}$LiFSI–TiO_2 (1 wt.%) electrolyte, this was for a much higher concentration of salt (188 mol%) and temperature (60 °C),[31] where the conductivity mechanisms are strikingly different than for low-to-moderate levels of salt. The high transference number obtained in this system could possibly be ascribed to that novel Li^+ transport routes at the surfaces of the ceramic filler appears by the addition of nanoparticles.[37] It has been argued before that the role of nano-fillers in SPEs are not solely limited to the prevention of polymer crystallization, but may also induce specific interactions via Lewis acid-base reactions between the filler surfaces and the polymer segments.[30] One reason for the very high cationic transference number obtained the P($CL_{80}TMC_{20}$)–$LiTFSI_{0.28}$-ZrO_2 system is therefore perhaps due to that Lewis acid groups on the filler surface compete with the Lewis acid of the lithium for the formation of complexes with the P($CL_{80}TMC_{20}$), thereby causing more free ions.[25] Such a phenomenon has also been observed in Density Functional Theory (DFT) calculations, where zirconia particles interacts with Li^+ cations by reducing their interactions with the polymer.[25] It can also be speculated that the TFSI anions can attract to nanoparticle surface functional groups via hydrogen bonding. This can also decrease the anionic mobility, and thereby increasing the cations transference number.

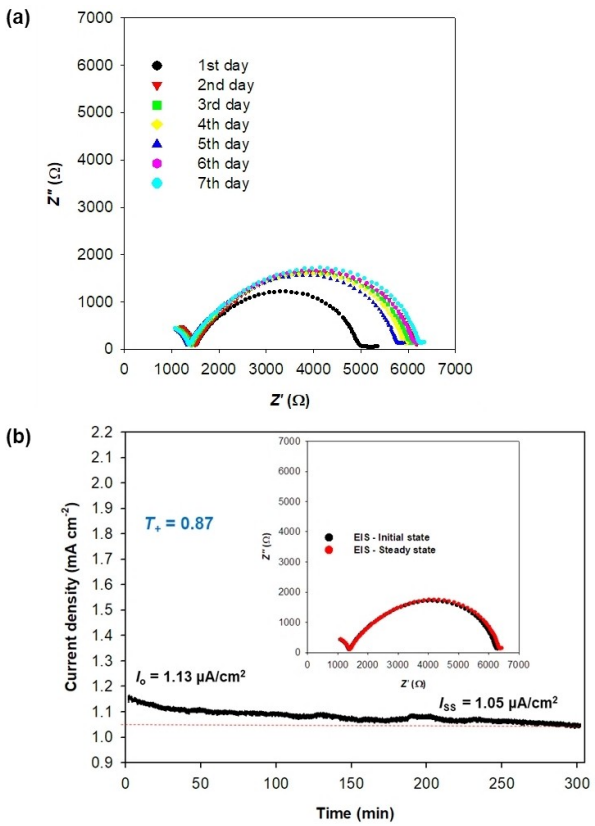

Figure 6. a) Interfacial resistances measured at different storage times and b) lithium transference number determination by potentiostatic polarization. Both samples are for the same symmetric Li/P($CL_{80}TMC_{20}$)–$LiTFSI_{0.28}$–ZrO_2/Li cell and data were obtained at 21–22 °C.

2.4.4. Half-Cell Battery Performance

To explore the electrochemical stability of the electrolyte in the actual electrochemical application, dynamic electrochemical

impedance spectroscopy (DEIS) was employed to study half-cell batteries. This method can determine the electrochemical responses of interfacial phenomena, where the variable frequency response of an AC signal is superimposed with a potentiodynamic DC voltage during a potential scan of a half-cell. Compared to the classical EIS method, this technique gives real-time information of interfacial processes (e.g. SEI formation) during charging or discharging. Hence, DEIS is an effective alternative tool to determine the R_{CT} values of the cell (at a stationary SOC) and is thus being useful for determining the cut-off limit for the battery cell. This is highly important to obtain the optimal performance of the cell, as shown by Matsumi and co-workers.[38–40] Figure 7 shows the DEIS profile of P($CL_{80}TMC_{20}$)–$LiTFSI_{0.28}$–ZrO_2 (4 wt.%) in a non-cycled half-cell battery which has been equilibrated for a week.

The changes in R_{CT} and R_b during cycling can be observed in Figure 7b. A sharp rise in R_{CT} at the initial potential (2.5 V) indicates primary formation of SEI layer. Upon charging to higher potentials, the R_{CT} gradually becomes lower and is stabilized at 3.8 V. However, the R_{CT} value rise again gradually after 4.0 V. Interestingly, the trend in R_b follows the R_{CT}, but in the opposite way: it displays an increase at 3.8 V and a subsequent decrease at higher potentials (above 4 V). Similarly, the current density recorded from the DEIS measurements (Figure 7c) is also increasing as R_{CT} is decreasing, which indicates that the increase of current is correlated to an increasing ionic transport at the electrode-electrolyte interface. After the optimum value of 3.9 V has been reached, the current density dropped again, indicating a decrease of ion transport.

Until recently, room-temperature operational all-solid-state lithium polymer batteries have largely been considered difficult to achieve, and cells have typically been cycled at elevated temperatures (55–80 °C).[11,36,41–43] In this context, we can show that this P($CL_{80}TMC_{20}$)-based nanocomposite polymer electrolyte holds potential to be employed as a true NCPE, which can be seen from the charge-discharge profile of the lithium half-cell assembled using of P($CL_{80}TMC_{20}$)–$LiTFSI_{0.28}$–ZrO_2 (4 wt.%) and cycled at or close to ambient temperatures (21–30 °C); see Figure 8. Based on the above DEIS analysis, the cut-off limits for the half-cell battery was set in between 2.6 to 3.9 V. In this temperature interval, when cycled galvanostatically at a current density of 0.032 $mAcm^{-2}$ (corresponding to C/10), the cycled cells showed useful discharge capacity of ca. 60 $mAhg^{-1}$ (21 °C) and ca. 100 $mAhg^{-1}$ (30 °C), respectively. The discharge capacity is gradually increasing as the cycling progresses, which can be attributed to improved interfacial contacts between the electrolyte and the electrode, as well as infiltration of NCPE into the porous electrode.[42,44] As a consequence, a fluctuating trend for the coulombic efficiency trends is seen,[18] although potential side-reactions can also explain this phenomenon. To further validate the capabilities of the cell, the lithium half-cell was also charged at higher potential up to 4.4 V (Figure S9); out of the optimum range indicated by DEIS analysis. The cycling data then shows that the capacity obtained is significantly higher (ca. 150 $mAhg^{-1}$), indicating large overpotentials in these cells. While this high capacity might seem encouraging, the capacity fading of the cell is inevitable (82% capacity retention after 55 cycles), likely due to that it is operating outside the electrochemical stability window of the electrolyte. Other strategies, such as optimizing the solid-state electrode, need to be employed in order to raise the capacity further. Unfortunately, cells were not able to cycle at higher temperature (> 40 °C), most likely due to too extensive softening of the SPE.

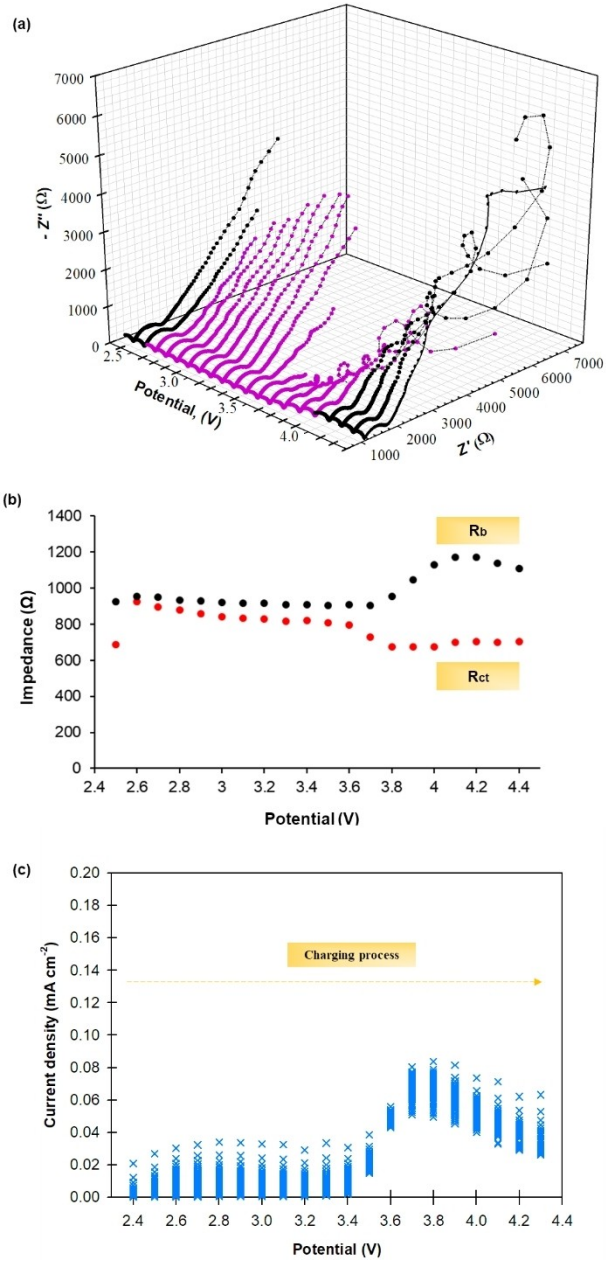

Figure 7. a) DEIS profile of a Li/P($CL_{80}TMC_{20}$)–$LiTFSI_{0.28}$–ZrO_2 (4 wt.%)/LFP cell, b) the R_{CT} and R_b plotted *vs* potential (impedance data fitted to a Debye circuit ($Q1/R1 + Q2/R2$) and c) current density *vs* potential derived from DEIS.

3. Conclusions

In this study, we have demonstrated that the organic-inorganic hybrid P($CL_{80}TMC_{20}$)–LiTFSI polymer electrolyte with zirconia

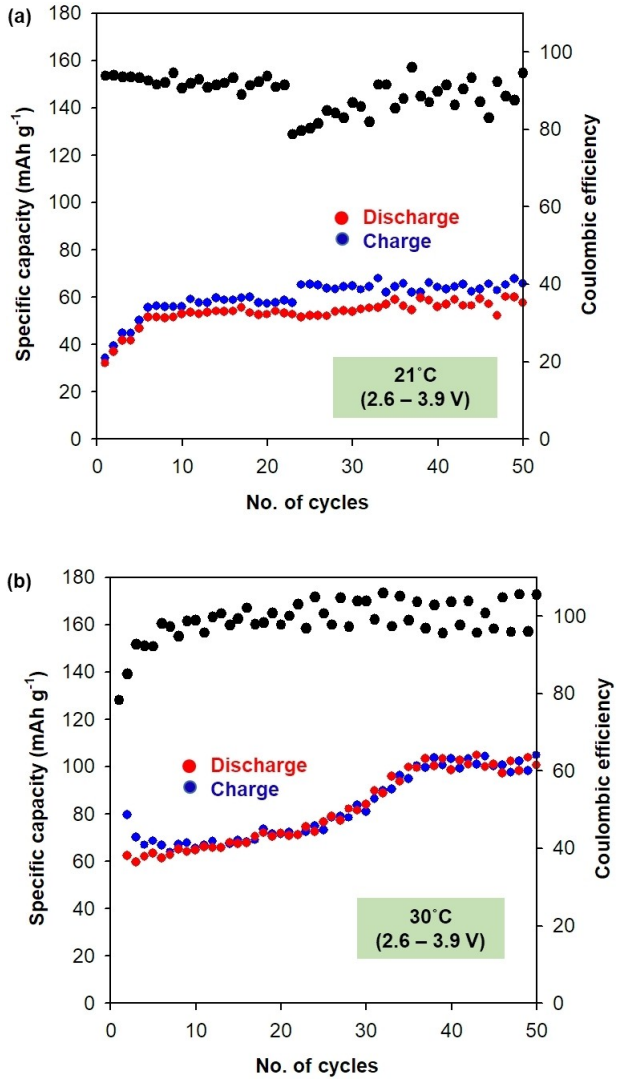

Figure 8. Charge-discharge galvanostatic profiles and coulombic efficiency of LFP half-cells using $P(CL_{80}TMC_{20})$–$LiTFSI_{0.28}$–ZrO_2 (4 wt.%) electrolytes in potential ranges of (a) 2.6–3.9 V at 21 °C and (b) 2.6–3.9 V at 30 °C.

nanoparticles is able to be used in all-solid lithium polymer batteries at ambient temperature with promising electrochemical properties. The inclusion of zirconia via an *in situ* sol-gel method enhanced the ion transport number and electrochemical stability of the $P(CL_{80}TMC_{20})$–LiTFSI material, possibly due to an alternative Li^+ pathway on the surface of the nanofiller or to anion-nanoparticle interactions. This ensured the formation of a more stable SEI layer, evident from stripping-plating lithium analysis. We also demonstrated that the *in situ* method of polymer electrolyte preparation with zirconia nanoparticles is feasible, and most importantly, enhanced several key properties of the polymer electrolyte as compared to the conventional casting methods. This will reduce the energy used to prepare the same sample, can lead to cost and time reductions in SPE preparation.

Experimental Section

Materials

ε-Caprolactone, CL (99%, Perstorp) was distilled under reduced pressure over CaH_2 whereas trimethylene carbonate (TMC; Richman Chemical) was used as received. Copolymers of 80 mol% ε-caprolcatone and 20 mol% trimethylene carbonate (denoted as $P(CL_{80}TMC_{20})$ were synthesized through bulk ring-opening polymerization according to previous published work[16]. Lithium (trifluoromethanesulfonimide) (LiTFSI; BASF) was dried in a vacuum furnace at 120 °C for 12 h prior to use. $LiFePO_4$ (LFP; Phostech Lithium), C-nergy super C65 Carbon Black (Imerys Graphite & Carbon), carbon-coated aluminum foil (Showa Denko), lithium foil (125 μm, Cyprus Foote Mineral Co.), nitric acid (65% HNO_3) (Merck) and zirconium (IV) propoxide (70%, Sigma-Aldrich) were purchased and used as received. All above chemicals except for HNO_3, $LiFePO_4$, current collectors and carbon black were handled and stored in a glovebox under argon condition. Other chemicals were obtained from commercial sources and used as received.

One-pot preparation of NCPE via *in situ* sol-gel method

Determined amounts of $P(CL_{80}TMC_{20})$ copolymer and LiTFSI salt were dissolved in anhydrous acetonitrile at 40 °C overnight. The solutions were allowed to cool down prior to synthesis of zirconia particles via an *in situ* sol-gel method. An amount of 10 μL of HNO_3 was added into the solution and stirred for 1 h before zirconium (IV) propoxide was added in dropwise. The controlled synthesis procedures were the same as described elsewhere, but without addition of ethanol[24–25]. The homogenous solutions were stirred for an hour before casting onto clean Teflon molds. The nanocomposite polymer electrolyte (NCPE) films were obtained by removing the solvent using a vacuum oven setup inside the glovebox where the samples were initially kept at ambient temperature while the pressure was gradually decreased from 200 mbar to <1 mbar during 20 h, followed by heating at 60 °C and <1 mbar for 40 h. After the drying process, the samples were punched into circular shape of 16 mm diameter for further use.

Characterizations

(a) Morphology observations – FIB-SEM

The morphology of the NCPE was studied using a FEI Strata DB235 dual beam FIB-SEM. A small layer of Pt coating was applied to reduce shadowing effects and charging. An energy beam of 2–5 keV was used. The zirconia nanoparticles synthesized without polymer was observed using a Zeiss Merlin scanning electron microscope (SEM) operating under a probe current of 5 keV.

(b) Molecular weight distribution

The molecular weight distribution of the polymers was determined through gel permeation chromatography (GPC) on a Verotech PL-GPC50 equipped with a refractive index detector and two Polar Gel-M organic GPC columns. THF was used as mobile phase eluent (35 °C, 1 ml min^{-1}) and calibration was done using narrow polystyrene standards. For detection, a viscometer detector was used. Prior to the analysis, the samples were diluted in THF and the solutions were filtered using through a 0.45 μm PVDF filter.

(c) Rheology analysis

Rheology measurements were performed on a Discovery Hybrid Rheometer (DHR 2, TA Instruments) with an 8 mm parallel plate geometry. The tests were ran at 25—100 °C for a frequency range of 0.01–10 Hz with an axial force of 1 N with 0.1 N tolerance. The samples were allowed to equilibrate for 5 min at each interval of temperature change.

(d) Ionic conductivity measurement

The ionic conductivity of the NCPE films was determined from the measured impedance using electrochemical impedance spectroscopy (EIS). The NCPE films (8–15 mm thickness) were sandwiched between stainless steel (SS) blocking electrodes and were sealed in standard CR2023 coin cells in a glovebox. Prior to measurement, the cells were equilibrated and heated to 100 °C for an hour in an oven where temperature was regulated by a thermocouple. The cells were then left to cool to room temperature overnight to allow for any possible recrystallization and ensuring good interfacial contact between electrolyte and electrodes. The EIS spectra were measured using an SI 1260 Impedance/Gain-Phase Analyzer (Schlumberger) at a frequency range of 1 to 10 MHz at an amplitude of 10 mV. The impedance was then obtained from the Nyquist plots by fitting to a Debye equivalent circuit to obtain the electrolyte resistance value. The ionic conductivity was calculated through from $\sigma = t/R_b A$ (**Eq. 1**), where t is the film thickness, R_b is the bulk resistance and A is the surface area of the electrode.

(e) Chronoamperometry

Based on the Bruce and Vincent's approach, the cation transference number (T_+) of the NCPE films was determined by potentiostatic polarization technique[45]. Symmetric Li/NCPE/Li cells were assembled inside coin cells and the impedance was monitored until a stable SEI was observed (no obvious change in resistance). Lithium was used as both working and counter electrode. Impedance and polarization measurements were carried out using a Biologic equipment (VMP2). The cells were polarized at 10 mV and the impedance spectra were obtained in the range 1–200 kHz. For polarization, the DC current was monitored as a function of time. All measurements were done at room temperature (23 °C).

(f) Cycling stability

Li symmetrical cell cycling tests were carried out using an Arbin BT2043 at room temperature. Galvanostatic cycles were run by applying 0.2 mA/cm^2 for 1050 cycles (1 h "plating" + 1 h "stripping" per cycle); equivalent to 2000 hours. Similarly, a series of different current densities (0.1–0.4 mA/cm^2) were employed for 20 cycles for each rate.

(g) Thermal properties

A TA instruments DSC Q2000 was used. The samples were hermetically sealed in aluminum pans in an argon-filled glovebox to avoid moisture absorption. To ensure an accurate comparison, each sample weight was approx. 6.5 mg. A cooling/heating-cooling/heating cycle was used from 25 to −80 °C before ramping to 100 °C with a ramping speed of 10 °C/min under a flow of N_2 gas. The second heating of the cycle was used to analyze the data.

(h) Battery cells

$LiFePO_4$ (LFP) cathodes were prepared from a slurry mixture of 80 wt.% of LFP active material powder, 10 wt.% carbon black and 10 wt.% of P($CL_{80}TMC_{20}$) as binder. The homogeneous slurry was deposited on a carbon-coated aluminum foil with a 150 μm film applicator (ZFR 2040 4-sided Applicator, Zehntner GmbH Testing Instruments). Prior to cell assembly, the electrodes were dried in a vacuum furnace at 120 °C for 12 hours, using an active mass loading ca. 1.81 mg cm^{-2}. All cells were fabricated and hermetically sealed in coin-cells (CR2025) in an argon-filled glovebox. Galvanostatic cycling of LFP/NCPE/Li half-cells was carried out on Novonix high precision (30 °C) and Arbin (room temperature) instruments between 2.6 and 4.4 V (extended range) and 2.6 and 3.9 V (limited range). All cells were pre-stored for 12 h before cycling.

Acknowledgements

This project has received funding from the European Research Council under grant agreement No. 771777 (FUN POLYSTORE). The authors also acknowledge support from STandUP for Energy and The Merdeka Award 2018 grant as well as Department of Chemical Sciences, Universiti Kebangsaan Malaysia (UKM). Dennis Karlsson and Isabell L. Johansson are acknowledged for assistance with the FIB-SEM treatment and GPC analysis, respectively.

Conflict of Interest

The authors declare no conflict of interest.

Keywords: zirconia nanoparticles · one-pot *in situ* preparation · poly(trimethylene carbonate)-ε-caprolactone · lithium transference number

[1] P. Yao, H. Yu, Z. Ding, Y. Liu, J. Lu, M. Lavorgna, J. Wu, X. Liu, *Front. Chem.* **2019**, *7*, 522.
[2] R. Chen, W. Qu, J. Qian, N. Chen, Y. Dai, C. Guo, Y. Huang, L. Li, F. Wu, *J. Mater. Chem. A* **2017**, *5*, 24677.
[3] The Nobel Prize in Chemistry 2019. NobelPrize.org. Nobel Media AB 2020. Thu. 2 Jan 2020. https://www.nobelprize.org/prizes/chemistry/2019/summary.
[4] M. Nojabaee, J. Popovic, J. Maier, *J. Mater. Chem. A* **2019**, *7*, 13331.
[5] E. P. Kamphaus, P. B. Balbuena, *J. Phys. Chem. C* **2017**, *121*, 21105.
[6] H. Zhang, X. Li, H. Zhang, *Li–S and Li–O_2 Batteries with High Specific – Energy Research and Development*, Gateway East, Singapore: SpringerBriefs in Molecular Science **2017**.
[7] W. Zhang, J. Nie, F. Li, Z. L. Wang, C. Sun, *Nano Energy* **2018**, *45*, 413.
[8] C. Sångeland, J. Mindemark, R. Younesi, D. Brandell, *Solid State Ionics* **2019**, *343*, 115068.
[9] C. Sun, J. Liu, Y. Gong, D. P. Wilkinson, J. Zhang, *Nano Energy* **2017**, 33, 363.
[10] K. Nie, Y. Hong, J. Qiu, Q. Li, X. Yu, H. Li, L. Chen, *Front. Chem.* **2018**, *6*, 616.
[11] Y. Zhao, Z. Huang, S. Chen, B. Chen, J. Yang, Q. Zhang, F. Ding, Y. Chen, X. Xu, *Solid State Ionics* **2016**, *295*, 65.
[12] W. Liu, N. Liu, J. Sun, P. C. Hsu, Y. Li, H. W. Lee, Y. Cui, *Nano Lett.* **2015**, *15*, 2740.
[13] P. Kurzweil, J. Garche, *Overview of Batteries for Future Automobiles*, Elsevier B. V., **2017**.
[14] Y. Zhao, C. Wu, G. Peng, X. Chen, X. Yao, Y. Bai, F. Wu, S. Chen, X. Xu, *J. Power Sources* **2016**, *301*, 47.

[15] T. Eriksson, J. Mindemark, M. Yue, D. Brandell, *Electrochim. Acta* **2019**, *300*, 489.
[16] J. Mindemark, E. Törmä, B. Sun, D. Brandell, *Polymer* **2015**, *63*, 91..
[17] D. Zhang, L. Zhang, K. Yang, H. Wang, C. Yu, D. Xu, B. Xu, L. M. Wang, *ACS Appl. Mater. Interfaces* **2017**, *9*, 36886.
[18] B. Sun, J. Mindemark, K. Edström, D. Brandell, *Electrochem. Commun.* **2015**, *52*, 71.
[19] Z. Li, R. Mogensen, J. Mindemark, T. Bowden, D. Brandell, Y. Tominaga, *Macromol. Rapid Commun.* **2018**, *39*, DOI 10.1002/marc.201800146.
[20] J. Mindemark, B. Sun, E. Törmä, D. Brandell, *J. Power Sources* **2015**, *298*, 166.
[21] Y. C. Jung, M. S. Park, D. H. Kim, M. Ue, A. Eftekhari, D. W. Kim, *Sci. Rep.* **2017**, *7* (1), 17482.
[22] F. Croce, L. Settimi, B. Scrosati, *Electrochem. Commun.* **2006**, 8, 364.
[23] W. Xiao, Z. Wang, Y. Zhang, R. Fang, Z. Yuan, C. Miao, X. Yan, Y. Jiang, *J. Power Sources* **2018**, 382, 128.
[24] L. Tiankhoon, N. H. Hassan, M. Y. A. Rahman, R. Vedarajan, N. Matsumi, A. Ahmad, *Solid State Ionics* **2015**, *276*, 72.
[25] L. T. Khoon, M. L. W. Fui, N. H. Hassan, M. S. Su'ait, R. Vedarajan, N. Matsumi, M. Bin Kassim, L. K. Shyuan, A. Ahmad, *J. Sol-Gel Sci. Technol.* **2019**, *90*, 665.
[26] O. Olea-Mejía, O. Olea-Cardoso, R. Lopez-Castañares, *Curr. Microsc. Contrib. to Adv. Sci. Technol.* **2012**, 1060.
[27] F. Croce, R. Curini, A. Martinelli, L. Persi, F. Ronci, B. Scrosati, R. Caminiti, *J. Phys. Chem. B* **1999**, *103*, 10632.
[28] I. Nicotera, L. Coppola, C. Oliviero, G. A. Ranieri, *Ionics (Kiel).* **2005**, *11*, 87.
[29] F. Harun, C. H. Chan, Q. Guo, *Macromol. Symp.* **2017**, *376*, 1700040.
[30] B. Scrosati, F. Croce, L. Persi, *J. Electrochem. Soc.* **2000**, *147*, 1718.
[31] Y. Tominaga, K. Yamazaki, *Chem. Commun.* **2014**, *50*, 4448.
[32] F. Croce, G. B. Appetecchi, L. Persi, B. Scrosati, *Nature* **1998**, *394*, 456.
[33] W. Wang, E. Yi, A. J. Fici, R. M. Laine, J. Kieffer, *J. Phys. Chem. C* **2017**, *121*, 2563.
[34] J. Popovic, D. Höfler, J. P. Melchior, A. Münchinger, B. List, J. Maier, *J. Phys. Chem. Lett.* **2018**, *9*, 5116.
[35] J. Zhao, J. Zhang, P. Hu, J. Ma, X. Wang, L. Yue, G. Xu, B. Qin, Z. Liu, X. Zhou, G. Cui, *Electrochim. Acta* **2016**, *188*, 23.
[36] K. Kimura, M. Yajima, Y. Tominaga, *Electrochem. Commun.* **2016**, *66*, 46.
[37] L. Chen, Y. Li, S. P. Li, L. Z. Fan, C. W. Nan, J. B. Goodenough, *Nano Energy* **2018**, *46*, 176.
[38] K. S. Smaran, P. Joshi, R. Vedarajan, N. Matsumi, *ChemElectroChem* **2015**, *2*, 1913.
[39] S. G. Patnaik, R. Vedarajan, N. Matsumi, *J. Mater. Chem. A* **2017**, *5*, 17909.
[40] A. Nag, M. A. Ali, A. Singh, R. Vedarajan, N. Matsumi, T. Kaneko, *J. Mater. Chem. A* **2019**, *7*, 4459.
[41] I. L. Johansson, D. Brandell, J. Mindemark, *Batteries and Supercaps* **2020**, *3*, 527.
[42] B. Sun, J. Mindemark, K. Edström, D. Brandell, *Solid State Ionics* **2014**, *262*, 738.
[43] J. Yang, X. Wang, G. Zhang, A. Ma, W. Chen, L. Shao, C. Shen, K. Xie, *Front. Chem.* **2019**, *7*, 388.
[44] B. Sun, I. Y. Liao, S. Tan, T. Bowden, D. Brandell, *J. Power Sources* **2013**, *238*, 435.
[45] J. Evans, C. A. Vincent, P. G. Bruce, *Polymer (Guildf).* **1987**, *28*, 2324.

Manuscript received: October 27, 2020
Revised manuscript received: November 26, 2020
Version of record online: December 29, 2020

